

Research Journal of Pharmaceutical, Biological and Chemical Sciences

Synthesis and characterization of pH-responsive nanocarrier based on PEGylated imidazolium ionic liquid MSN@GO for in-vitro curcumin delivery.

Reza Rahmatolahzadeh ^a, Masood Hamadian ^{a,*}, Leila Ma'mani ^b, Abbas Shafiee ^c

^aInstitute of Nano Science and Nano Technology, University of Kashan, Islamic Republic of Iran.

^bDepartment of Nanotechnology, Agricultural Biotechnology Research Institute of Iran (ABRII), Agricultural Research, Education and Extension Organization (AREEO), Karaj, Islamic Republic of Iran.

^cDepartment of Medicinal Chemistry, Faculty of Pharmacy and Pharmaceutical Sciences Research Center, Tehran University of Medical Sciences, Tehran 14176, Islamic Republic of Iran.

ABSTRACT

PEGylated imidazolium ionic liquid functionalized MSN@GO (PEGylated ImIL functionalized MSN@GO NPs) has been fabricated and evaluated as a pH-responsive drug carrier for delivery of curcumin. The Poly ethylene glycol is decorated onto the surface of MSN@GO to enhance its stealth during blood circulation. The standard techniques such as X-ray powder diffraction (XRD), dynamic light scattering (DLS), UV-Vis spectroscopy, thermal gravimetry analysis (TGA), FT-IR, and scanning and transmission electron microscopy (SEM & TEM) were applied for characterization of nanocarrier. The size of MSN@GO based nanocarrier and the amount of loaded CUR were around 166 nm and 16.4 % w/w of nanocarrier, respectively. The cumulative drug release amounts were obtained 52% and 92% at pH 7.4 and 5.8, respectively. The MSN@GO based nanocarrier had no cytotoxicity against normal, human breast adenocarcinoma (MCF-7) and human mammary epithelial (MCF10A) as cancerous and normal cell lines. Whereas the curcumin loaded PEGylated ImIL functionalized MSN@GO NPs showed excellent killing capability against MCF-7 cells. Flow cytometry analysis was used to measure the cellular uptake of curcumin@[PEGylated imidazolium ionic liquid MSN@GO] NPs.

Keywords: Breast cancer, PEGylated ImIL functionalized MSN@GO, Mesoporous silica nanoparticles, pH-Responsive.

**Corresponding author*

INTRODUCTION

Due to the importance of breast cancer, known as carcinoma of the breast, as the most common type of cancer in women a large numbers of researches have been devoted to develop efficient and impressive drug delivery systems (DDSs) for anticancer transport and delivery to the cancer cells [1,2]. Graphene as a layered structure with a structure of hexagonal cell has shown high possible for applying in biosensors, nano-electronic, and transparent electrodes [3]. Also, owing to the high matrix efficiency and high specific surface area (theoretical value $2630 \text{ m}^2 \text{ g}^{-1}$), it is a robust and promising candidate as a sorption material [4,5]. Graphene oxide (GO), the oxidized counterpart of graphene, contains carboxyl and hydroxyl functional groups which can be functionalized with biomolecules and drugs for *in vitro* and *in vivo* biological applications [6-7]. Curcumin (CUR), a natural diphenolic compound derived from turmeric *Curcuma longa* L. (Zingiberaceae family) rhizomes], has valuable pharmaceutical properties such as anti-cancer, anti-inflammatory, anti-microbial, anti-oxidant, and anti-fungal activities [8-12]. But the utilization of CUR as a hydrophobic drug, in pharmaceutical applications is limited by some disadvantage including poor bioavailability, low solubility, absorption complicated with a high first-pass, and rapid elimination. Exploiting the therapeutically activities of CUR have serious challenges hence, a large number of efforts have been allocated to develop an efficient nano-DDS for efficient CUR transport and delivery [13,14]. Mesoporous silica nanoparticles (MSNs) occupy a unique global niche as “reliable support or carrier materials” and due to their efficiency they have attracted a great deal of attention for their potential biomedical applications [15]. The useful MSNs’ features including ordered structure with high pore volume and surface area accompanied hydrothermal stability, biocompatibility give us outstanding and valuable opportunities for designing beneficial DDSs [16]. Recently, graphene–mesoporous silica composites have been prepared, which the silica component consisted of a smooth uniform coating. The mesoporous material was dispersed into the surface of the graphene sheets, not only could the graphene and the porous material maintain the inherent characteristics of each, but also produced a novel synergistic effect [17-20]. The ability of tailoring its numerous end groups offers considerable scope for fine-tuning its drug loading and targeted release properties. Drug targeting to cancer cells is an interesting task [21-24]. Due to the excellent aqueous solubility, biocompatibility, non-toxicity, non-antigenic, and non-immunogenic characteristics, poly (ethylene glycol) (PEG) is used as a well-established surface modifying agent [25,26]. And covalently PEGylation has been increasingly considered to reducing the blood interaction (low plasma protein binding) and also as a suitable manner to enhance the permeability, retention effect, EPR effect, and colloidal stability in aqueous medium [27]. The aforementioned facts have been encouraged the researchers to attempt for developing a novel, low-cost and more efficient DDS based on MSN and GO scaffolds having various surface characteristics. Therefore, considering the valuable pharmaceutical activities of CUR and also in continuation of our pervious experiences in the field of nanoporous materials [28], we present an efficient MSN@GO based nano-DDS to improve the loading and therapeutic effect of CUR. It was exploitable that the PEGylated imidazolium ionic liquid functionalized MSN@GO NPs (PEGylated ImIL functionalized MSN@GO NPs) performs as a worthy candidate for the *in vitro* cancer treatment.

EXPERIMENTAL

Materials

Poly (ethylene glycol) (PEG) (Mw = 600), 4-Toluenesulfonyl chloride, Tetraethyl orthosilicate (TEOS, 98%), 3-(4,5-Dimethylthiazol-z-yl)-2,5-diphenyltetrazotium bromide (MTT), dimethyl sulfoxide (DMSO) and highly purified curcumin were purchased from Sigma. Phosphate buffer (20 mM, pH 7.8) and corresponding salts were used throughout this research, and EDTA was purchased from Merck. Trypsin, culture medium (DMEM= Dulbecco’s Modified Eagle’s Medium), and supplements were obtained from Gibco (Germany). MCF-7 (human breast adenocarcinoma) was purchased from Pasteur Institute (Tehran, Iran). The cell lines were grown in DMEM medium supplemented with 10% (v/v) heat-inactivated fetal bovine serum (FBS), 2% l-glutamine, 2.7% sodium bicarbonate, 1% HEPES buffer, and 1% penicillin-streptomycin solution (GPS, Sigma) at 37 °C in humidified atmosphere with 5% CO₂. All cells were trypsinized in the solution of 0.05 % trypsin and seeded into 96-well micro-plates at the density of 1×10^5 cells/well.

Characterization

The powder XRD spectrum was recorded at r.t. with a Philips X’pert 1710 diffractometer using CuK α ($\alpha = 1.54056 \text{ \AA}$) in the Bragg-Brentano geometry (θ -2 θ). The morphologies of the products were observed using

SEM (Hitachi S-4800 II, Japan) equipped with energy dispersive X-ray spectroscopy. Ultraviolet–visible spectra of NPs were recorded using UV–Vis Jasco-530. The TEM experiments were performed on a Hitachi H-7650 (Tokyo, Japan) operating at an acceleration voltage of 80 kV. The IR spectra were taken using Nicolet FT-IR Magna 550 spectrographs with spectroscopic grade KBr. The surface areas were calculated by BET method and the pore size distributions were calculated from the adsorption branch of the isotherms using BJH method. The size of the NPs was assessed by dynamic light scattering (Nano-ZS 90, Malvern Instrument, United Kingdom). The zeta potential of the NPs was calculated in folded capillary cells (ZetasizerNano ZS90 (Malvern Instruments Ltd., Malvern, UK)).

Preparation of nanocarrier

Preparation mesoporous silica nanoparticle-graphene oxide hybrid (MSN@GO)

Graphitic oxide structure (GO) was obtained according to our prior report through the modified Hummers method [29]. Briefly, GO powder (1 g) was appended to a solution of H₂SO₄ (50 mL 96%) in an ice bath and KMnO₄ (2 g) was added to solution. The reaction mixture was left to flick for 3 h < 10 °C, and continued by another 30 min at 35 °C. Then the product obtained was diluted with deionized water (DW, 50 mL) where the temperature was kept <100 °C. After 30 min of shaking, the product obtained was further diluted to 100 mL with water. And, H₂O₂ 30% (10 mL) was added to the mixture. The final solid was separated and washed thoroughly with 5% Hydrochloric acid aqueous. At the end the resultant was dried at 70 °C for 48 h. Then, MSN@GO hybrid was synthesized using GO and TEOS, according to the previous report with slight modification [30]. Typically, a solution of CTAB (8 g) and sodium hydroxide (0.2 g) in 400 mL DW was combined to a suspension containing 450 mg of GO (pH = 8.5). Then TEOS (6 mL) dissolved in EtOH (10 mL) was added drop-wise to the later mixture and allowed to stir at 70 °C for 12 h. The resulting product was centrifuged and washed thoroughly applying soxhlet with EtOH/HCl (1%). MSN@GO fine powder obtained after drying the solid residual in a vacuum oven at 30 °C overnight.

Preparation of PEGylated mesoporous silica graphene oxide

To prepare PEGylated MSN@GO, PEG-silane as a linker was synthesized according to our previous report [32]. Then a solution of PEG-silane (2 g) in 25 mL of pure EtOH was added dropwise to an intense stirring solution of MSN@GO (0.5 g) in 25 mL EtOH/H₂O (1:3) and HCl (pH = 3.5). After stirring for 12 h, the Previous solution was filtered off and washed thoroughly with H₂O/EtOH. As a result, The resulting solution was dried at 60 °C in vacuum to obtain PEGylated MSN@GO.

Synthesis of PEGylated ImIL functionalized MSN@GO NPs

At the first, 10 g of PEGylated MSN@GO was dissolved into solution of water and H₂SO₄ (100/ 4 mL) and then 20 g of HBr is dissolved in 50 mL of water and is added drop-wise to the later solution and the reaction was stirred at 100 °C for 18 h. At the end of time, Neutralize acidic solution was made by adding sodium hydroxide. At the following, the resulting solution was filtered off, then remove the solvent to obtain brominated of MSN@GO-PEG-Br. Then, 2 mL triethylamine was added to MSN@GO-PEG-Br solution (4 g in 40 mL EtOH) and then stirred for 10 min. at 20 °C and N-methylimidazol (2 mmol) was reacted with a solution of PEG. After 24 h of reaction time at 25 °C, the The resulting solution was washed with water (2 x10 mL), filtered and dried under vacuum to obtain PEGylated MSN@GO imidazolium ionic liquid.

Preparation of drug-loaded NPs

In order to investigate the loading capability, a CUR solution was added to a 20.0 mg of CUR@[PEGylated ImIL functionalized MSN@GO] NPs in acetone and put under Argon atmosphere overnight. In the following, the solid was obtained by centrifugation at 11,000 rpm. Then unlinked CUR remove by washing with EtOH and dried to give CUR@[PEGylated ImIL functionalized MSN@GO] NPs. The residual CUR content Calculated by UV-Vis measurement of the extracted from both of the supernatant and washed solutions, the loading efficiency was achieved.

Drug release investigation

The release of CUR from PEGylated ImIL functionalized MSN@GO NPs was measured at predetermined time points (0-120 h). To investigate the in vitro release of Phosphate buffer solution (pH 7.4 and 5.8) were used as normal and acidic pH at 37°C, respectively. Therefore, 10.0 mg of the CUR@[PEGylated ImIL functionalized MSN@GO] NPs was entranced to a dialysis bag with cut-off 3500 g.mol⁻¹ and soaked into 200 mL of phosphate buffer solution (PBS) (0.01 M, pH = 7.4 and 5.8). Sampling of solution buffer was carried out in 0, 2, 4, 8, 12, 24, 36, 48, 72, 96, and 120 h. After each sampling, 1.0 mL of samples was collected and the medium was changed with 1.0 mL of the same fresh buffer solution. At the following, for determine the amount of the released CUR was used fluorescence spectroscopy (450 nm).

Designation of drug loading and encapsulation efficiency

Dissolution method was used to determination curcumin content in the nanocarrier by application of Beer's law. 20 mg of CUR@[PEGylated ImIL functionalized MSN@GO] NPs was dissolved in 10 mL of acetone and ethanol. UV-Vis absorption was used for determination concentration of CUR at their maximum wavelength (432 nm). The following equations was used to Designation of drug loading (DL) and Encapsulation efficiency (EE) (Eqs. (a) and (b)):

$$DL(\%) = \frac{\text{Weight of encapsulated curcumin}}{\text{Weight of tht nanoparticles}} \times 100 \quad \text{Eq. (a)}$$

$$EE(\%) = \frac{\text{Weight of encapsulated curcumin}}{\text{Total weight of curcumin}} \times 100 \quad \text{Eq. (b)}$$

The measurement of Particle size and zeta potential

Dynamic light scattering (DLS) is a non-invasive technique for measuring the size of particles and molecules in suspension, DLS and zeta-potential measurements have the potential to determine the size distribution, average size, and charge distribution of the freeze-dried CUR@[PEGylated ImIL functionalized MSN@GO] NPs.

Physical stability of CUR@[PEGylated ImIL functionalized MSN@GO] NPs under physiological condition

The physical stability of the CUR@[PEGylated ImIL functionalized MSN@GO] NPs was tested in media at pH 7.4. The particle sizes of CUR@[PEGylated ImIL functionalized MSN@GO] NPs were determined by DLS technique. The average hydrodynamic diameter of NPs was measured with sampling at 0, 2, 4, 6, 8, 12, 16, 24, 48, and 72 h.

A method of Cell Viability Assay

The cytotoxicity of CUR, PEGylated ImIL functionalized MSN@GO, and CUR@[PEGylated ImIL functionalized MSN@GO] NPs were investigated in MCF-7 and MCF10A as cancerous and normal cell lines, respectively, the colorimetric analysis was used to measure the reduction of MTT. Cells (1×10^4) were seeded in 80-well plates. The dried CUR@[PEGylated ImIL functionalized MSN@GO] NPs were suspended in medium and then added to the cells. After 24 h, diverse concentrations of samples (CUR, PEGylated ImIL functionalized MSN@GO, and CUR@[PEGylated ImIL functionalized [MSN@GO] NPs) were applied. After 12, 24, 48, 72 and 120 h of exposure, the cells were washed twice with PBS and then 20 μ L of MTT was added to each well. Then NPs incubated plates for 4 h at 37 °C. The results were analysed.

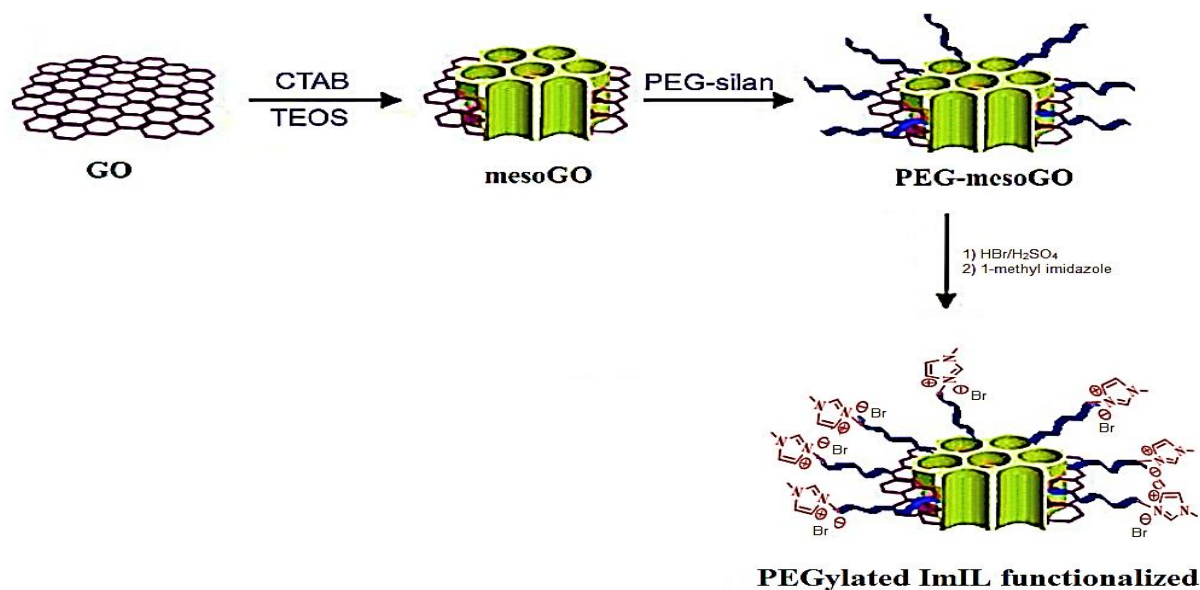
Cellular uptake

The cellular uptake of CUR@[PEGylated ImIL functionalized MSN@GO] NPs in MCF-7 human breast adenocarcinoma cells were studied with 2×10^5 cells in 5-well plates in medium (DMEM). At certain times media was replaced with 2 mL of serum-free medium containing CUR loaded NPs. The cells were washed twice with PBS Then The results were analysed with the spectrofluoro photometer.

RESULTS AND DISCUSSION

Illustration of drug delivery system

The simple and quantitative synthetic approach for the preparation of the designed nano-carrier CUR@[PEGylated ImIL functionalized MSN@GO] NPs is shown in Scheme 1. The synthesized porous frameworks were characterized by XRD, N₂ adsorption-desorption analysis, FT-IR, TGA, TEM, and SEM. As shown in Fig. 1a and b, the synthesized mesoporous-graphene based NPs possess a porous framework. Additionally, TEM images illustrated that mesoporous silica were widely covered with thin transparent GO sheets, which demonstrated that the modified GO is highly ordered. The SEM images of MSN@GO and PEGylated ImIL functionalized MSN@GO NPs are shown in Fig. 2, (a,b). The FT-IR spectra of the MSN@GO, PEGylated ImIL MSN@GO and CUR@[PEGylated ImIL functionalized MSN@GO] NPs (Fig. 3). In Fig. 3a, FT-IR spectra of PEG-silane reveals the broad band at 1113 cm⁻¹ which is related to the C–O bond of PEG segment and Si–O bond, and the peak at 2885 cm⁻¹ results from the methylene group. The broad peaks at 1715 and 3410 cm⁻¹ are due to C=O bond and hydroxyl groups in PEG, respectively. While the characteristic peak at 1390 and 1568 cm⁻¹ are assigned for the presence of C–N and N–H bonds in PEG-silane, respectively. In Fig. 3b, FT-IR spectra of PEGylated ImIL reveals the broad C–O–C band at 1099 cm⁻¹ is related to the etheric linkages of PEG segment and the peak at 2874 cm⁻¹, result from the methylene group near to oxygen atom. The broad peak at 3489 cm⁻¹ is due to the O–H and N–H stretching band of the end hydroxyl and amine groups in PEGylated ImIL, while the characteristic peak at 1377 cm⁻¹ is assigned for the presence of C–N bond in the imidazole and 1594 cm⁻¹ related to N–H bend, the C=C aromatic at 1644 cm⁻¹. In Fig. 3c, FT-IR spectra CUR@[PEGylated ImIL functionalized MSN@GO] NPs have different peak than [PEGylated functionalized ImIL]. New peaks are indicating the changes in the structure after the reaction with CUR. The mesoporous-graphene hybrid framework was assessed by XRD experiment. As seen in Fig. 4a, the low angle XRD pattern is confirmed the mesoporous matrix. The XRD patterns show that the peak positions have virtually fixed that confirm the retention of the GO scaffold after the manipulation (Fig. 4b). To assay the surface nature of the NPs, the N₂ adsorption–desorption isotherm experiment was done (Fig. 5). The specific surface area, diameter distribution, and total pore volume for solids were measured by the multiple-point BET (Brunauer, Emmett and Teller) and BJH (Barrett–Joyner–Halenda), respectively. The surface area, pore volume, and pore size has decreased after surface functionalization (Table 1). The thermogravimetric plots for hybrid of MSN@GO samples, which are all characterized by a mass loss step in the 600 °C region. In Fig. 6, the TGA analysis of samples showed a first peak at 100 °C which related to desorption of water and second peak at all samples are related to loss of the organic group. Based on these results, it is found that the loading of PEG was 42% w/w. The amount of PEGylated ImIL moieties loaded into MSN@GO scaffold was also confirmed by elemental analysis. Also the TGA analysis of CUR@[PEGylated ImIL functionalized MSN@GO] NPs showed the weight loss of about 69 %, which could be related to the elimination of CUR and PEG linker.



Scheme 1. Synthesis of CUR@[PEGylated ImIL functionalized MSN@GO] NPs.

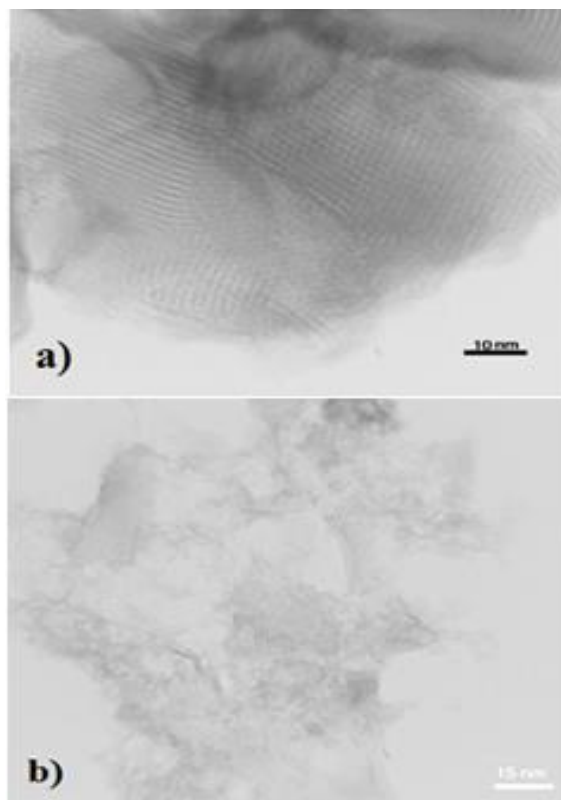


Fig. 1 Fig. 1.TEM of a) MSN@GO, b) PEGylated ImIL functionalized MSN@GO NPs.

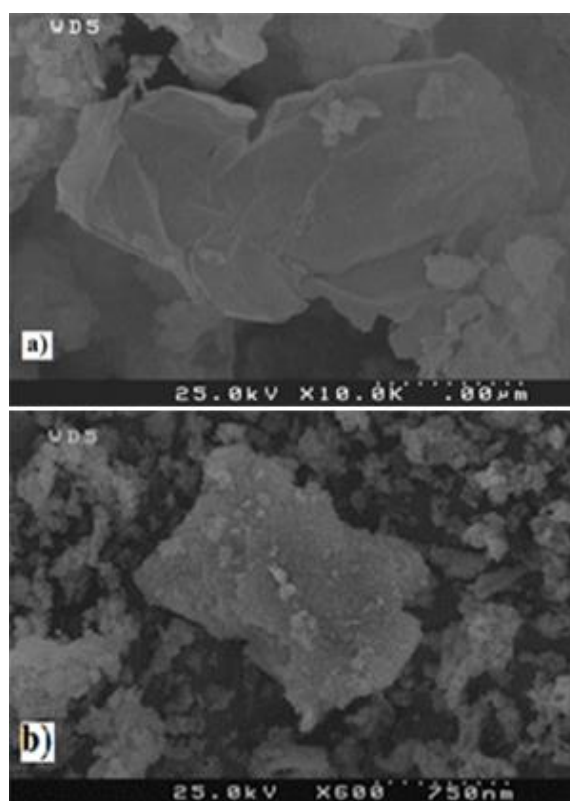


Fig. 2. FESEM of a) MSN@GO, b) PEGylated ImIL functionalized MSN@GO NPs.

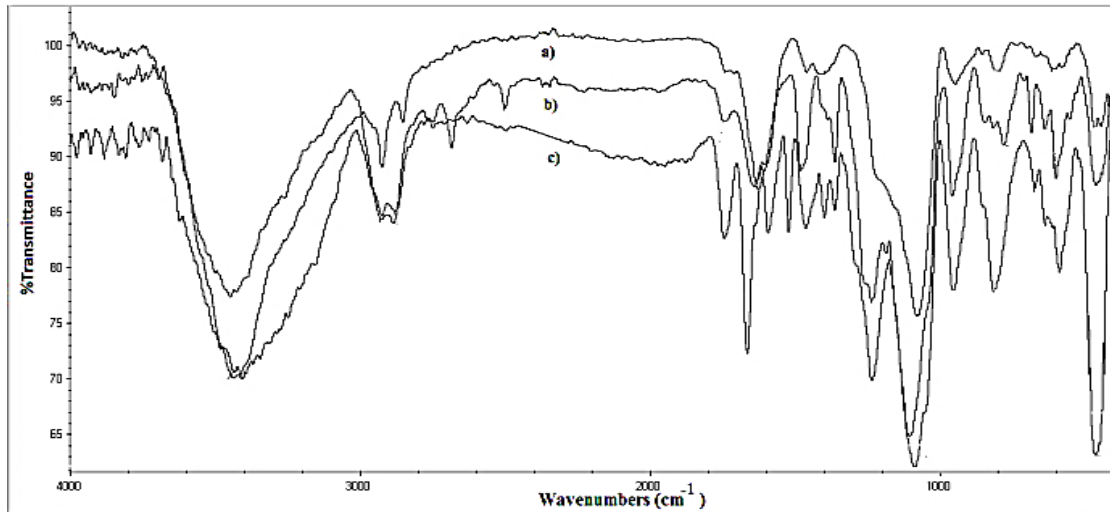


Fig. 3. FT-IR spectra of a) MSN@GO, b) PEGylated ImIL functionalized MSN@GO, and c) CUR@[PEGylated ImIL functionalized MSN@GO] NPs.

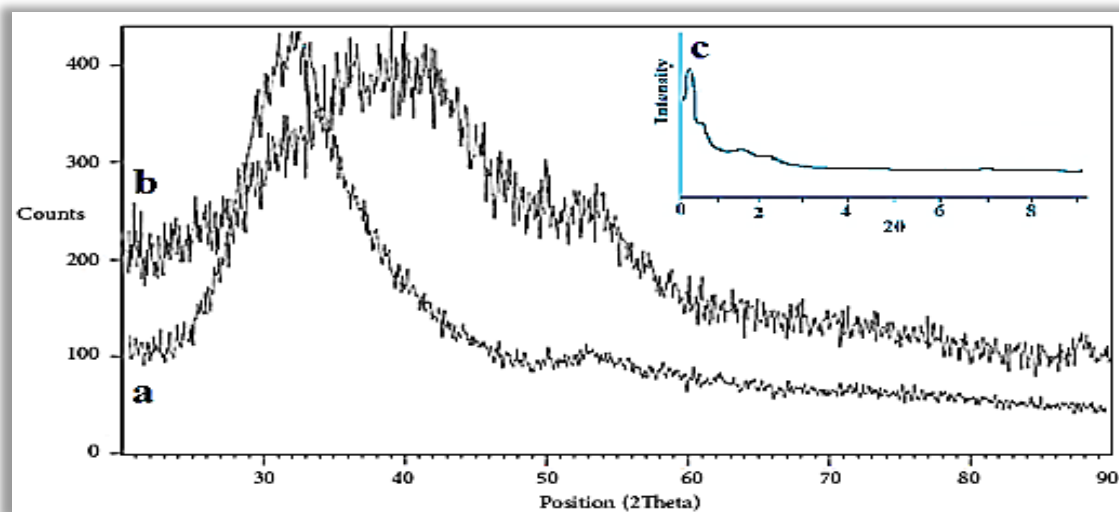


Fig. 4. The XRD patterns of a) GO, b) GO@MSN, c) low angle XRD of MSN@GO, respectively.

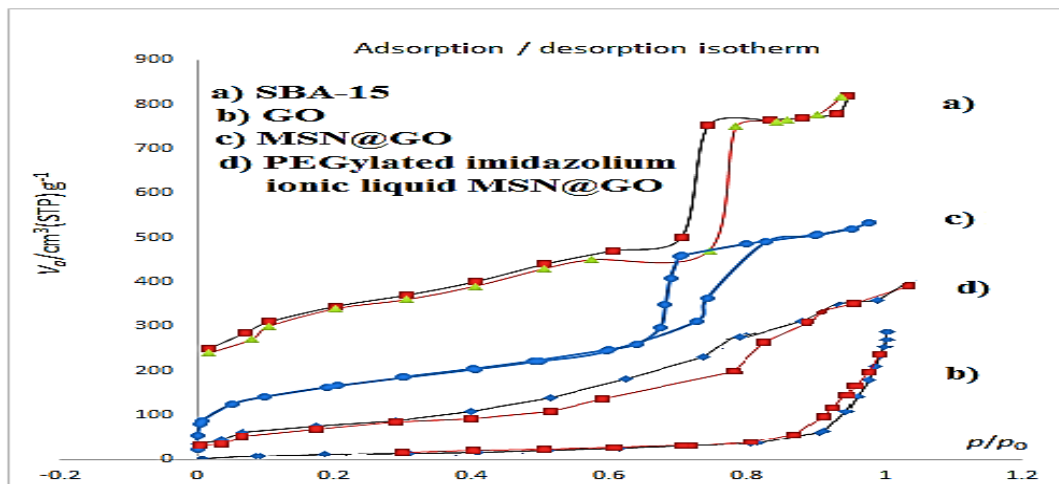


Fig. 5. Nitrogen adsorption – desorption isotherm pattern a) SBA-15, b) GO, c) MSN@GO, d) PEGylated ImIL functionalized MSN@GO NPs.

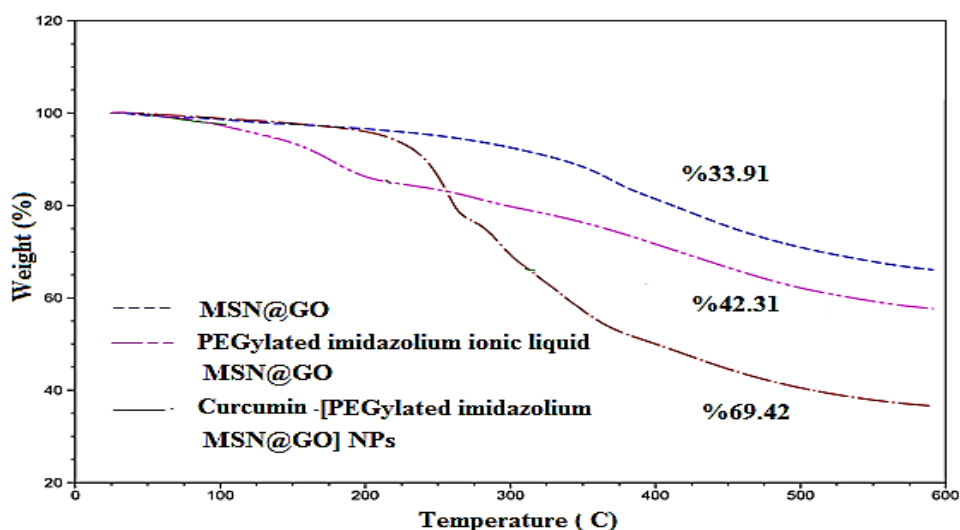


Fig 6. TGA of a) MSN@GO, b) PEGylated ImIL functionalized MSN@GO, and c) CUR-[PEGylated ImIL functionalized MSN@GO] NPs.

Table 1. BET and BJH analysis for MSN@GO based materials

NPs	S_{BET} (m^2g^{-1})	V_{total} ($cm^3.g^{-1}$)	Pore diameter (nm) (BJH)
GO	110	0.219	10.20
MSN@GO	560	0.589	8.9
CUR@[PEGylated ImIL MSN@GO]	210	0.243	3.5

The particle size distributions of CUR-[PEGylated ImIL functionalized MSN@GO] NPs in PBS solution determined using DLS is relatively narrow (mean diameter = 166 nm, PDI = 1. Therefore, PD index shows that the MSN@GO has uniform distribution, which is considered as a critical factor in biomedicine applications. The zeta potential for PEGylated ImIL functionalized MSN@GO NPs is negative (-24.1 mV) that zeta potential measurements showed that after PEGylated ImIL functionalization and CUR loading the zeta potential is changed to positive amounts.

Determination of CUR loading efficiency

To achieve the optimal loading efficiency for the designed nanocarrier, different ratios of PEGylated ImIL functionalized MSN@GO NPs and drug were assessed to achieve the desirable efficiency in loading. The obtained mixtures were centrifuged at 12000 rpm and supernatant harvested completely. The amount of CUR remaining in the collected supernatant was then measured by a spectrophotometer at 432 nm. The loading efficiency of CUR@[PEGylated ImIL functionalized MSN@GO] NPs was $64 \pm 1.5\%$ with proportion of 1:1.5 for PEGylated ImIL functionalized MSN@GONPs /CUR.

In-Vitro Release of CUR

The amount of released CUR from CUR@[PEGylated ImIL functionalized MSN@GO] NPs were determined by measuring the fluorescence emission intensity of the supernatant under different pH (7.4 and 5.8). The pH values 7.4 and 5.8 indicate the pH of normal blood and cancerous cells environment, respectively. According to the release curves (Fig. 7), CUR has been released from CUR@[PEGylated ImIL functionalized MSN@GO] NPs over a 100 h period with a slower release pattern at pH 7.4 in comparison to pH 5.8. The results show a CUR release efficiency about 40.49% and 68% under physiological and acidic condition from CUR-[PEGylated ImIL functionalized MSN@GO] NPs at the first 24 h which are uniformly increased and reached to about 56% and 90% after 100 h under normal and acidic conditions, respectively. These results demonstrate that the releasing profile of CUR under acidic condition is much higher than normal pH, that it is shown the CUR-[PEGylated ImIL functionalized MSN@GO] NPs will be more efficient in cancerous cell environments.

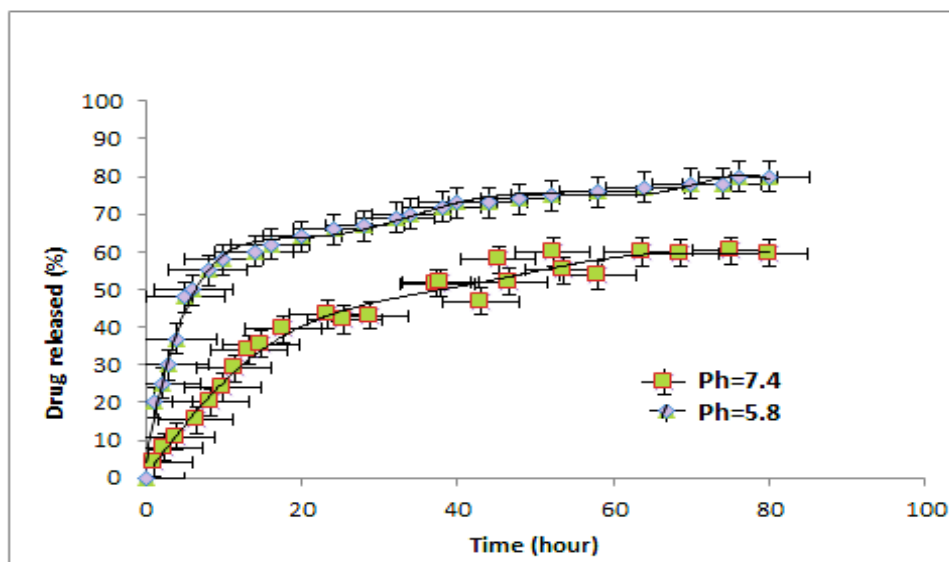


Fig. 7. *In vitro* release profiles of CUR@[PEGylated ImIL functionalized MSN@GO] NPs at pH 7.4 and pH 5.8; all experiments were performed at 37°C. Data represent mean values ± SD (n = 3).

Cell Viability

The in-vitro investigation of the toxicity of CUR@[PEGylated ImIL functionalized MSN@GO] NPs in the case of MCF-7 cancerous cell lines as well as MCF10A were carried out using MTT assay (Fig. 8). CUR@[PEGylated ImIL functionalized MSN@GO] The IC50 value of CUR@[PEGylated ImIL functionalized MSN@GO] NPs for MCF-7 cell lines within 12, 24, and 48 h were 30, 21.5 and 15 μM, respectively which reduced to 14 μM in 72 h. In contrast, the same concentrations of CUR@[PEGylated ImIL functionalized MSN@GO] NPs did not affect the proliferation of MCF10A cells that verifies the safety and biocompatibility of CUR@[PEGylated ImIL functionalized MSN@GO]NPs.

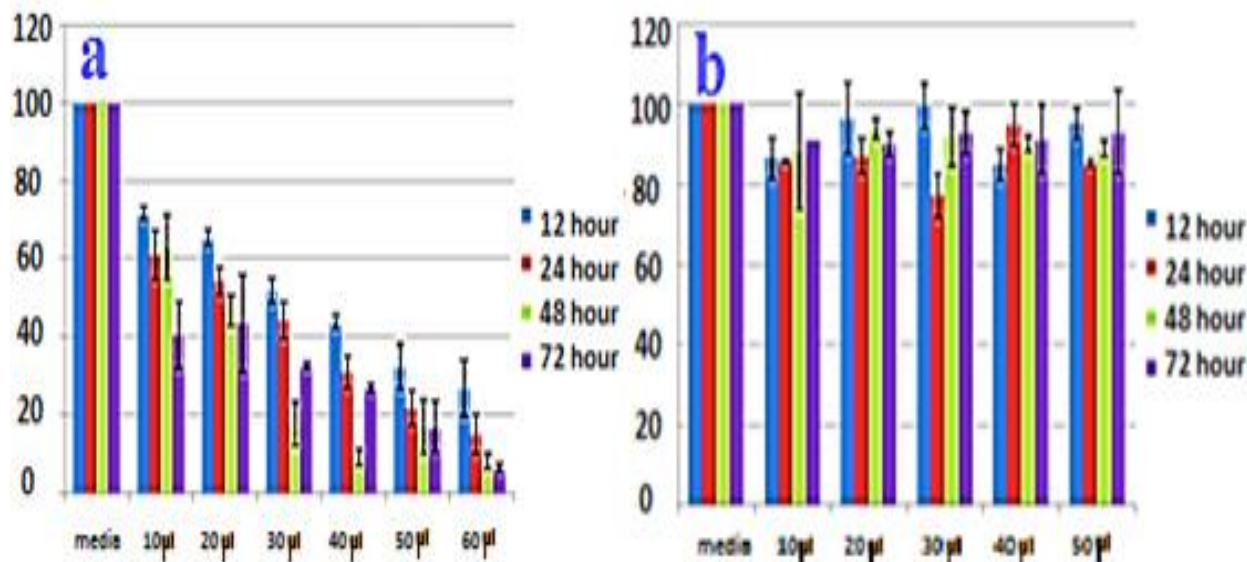


Fig. 8. The cytotoxicity effects of CUR@[PEGylated ImIL functionalized MSN@GO] NPs on (a) MCF-7 and (b) MCF10A.

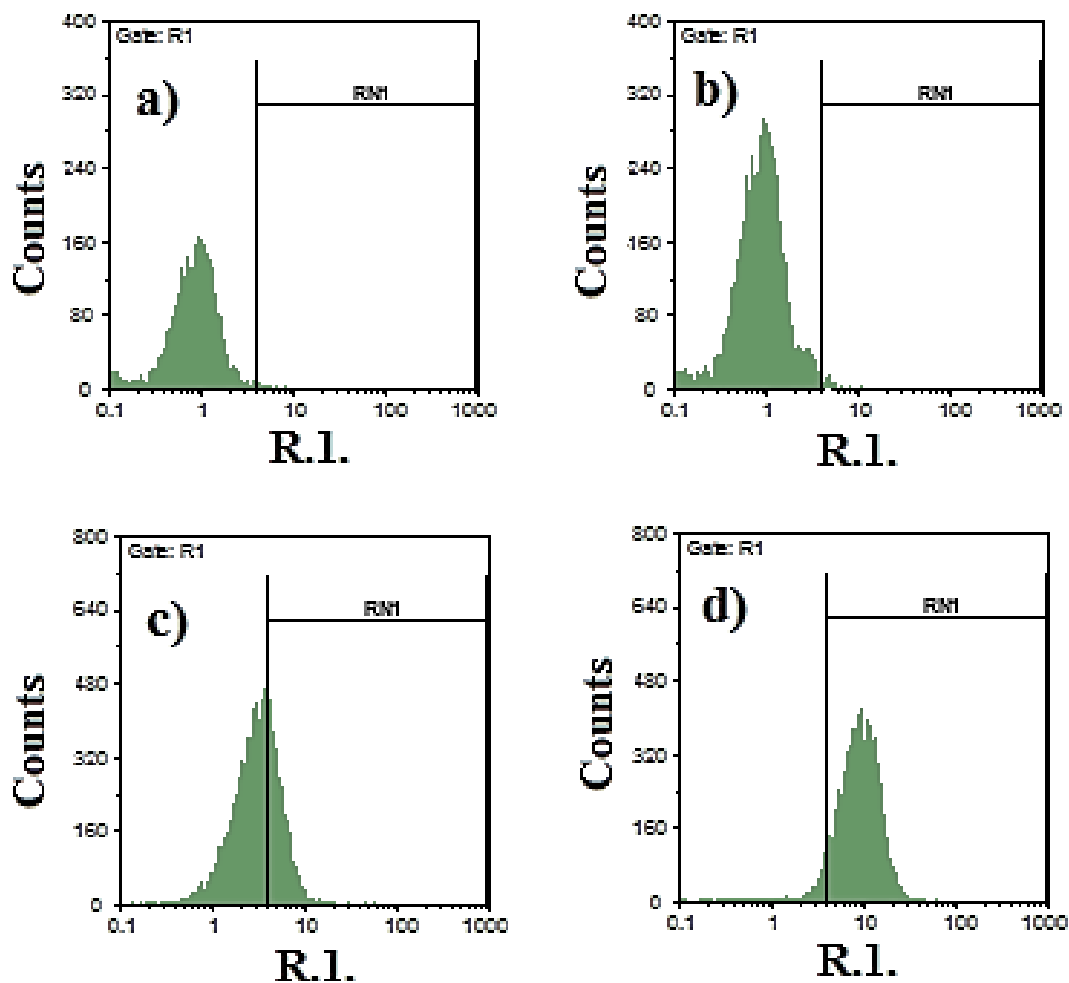


Fig. 9. Cellular uptake of CUR and CUR loaded NPs by flow cytometry. a) autofluorescence of MCF-7 cells; b) CUR; c) MCF-7 cells incubated with CUR; d) MCF-7 cells incubated with CUR@[PEGylated ImIL functionalized MSN@GO] NPs.

Cellular uptake of NPs

The uptake quantitative analysis of NPs by flow cytometry (Fig. 9) shows the histograms of cellular fluorescence for CUR, and MCF-7 cells incubated with and without CUR loaded NPs. The cells without CUR and NPs which used as a negative control show only auto-fluorescence Fig. 9a and b. Strong CUR fluorescence was observed when MCF-7 cells were incubated with CUR (Fig. 9c), and MCF-7 cells incubated with CUR loaded [As-PEGylated MSN@GO] NPs (Fig. 9d), respectively. A higher uptake of CUR loaded NPs in breast cancer cells could be an indication for an improved therapeutic index.

CONCLUSION

Herein, a PEGylated functionalized mesoporous silica nanoparticles-graphene oxide hybrid has been fabricated by anchoring ImIL and PEG functional moieties onto the surface of MSN@GO scaffold as a biocompatible and water-dispersed nanomaterial. Then it has been evaluated as nanocarrier for improving the delivery of CUR to cancerous cell lines. Indeed the structure of ImIL functionalized PEGylated MSN@GO nanocarrier was fully characterized and confirmed by a variety of techniques. Then CUR was loaded on the surface of the modified MSN@GO NPs. MTT assay technique was applied to examine the efficiency of CUR@[PEGylated ImIL functionalized MSN@GO] NPs as anticancer. Our data suggest that CUR@[PEGylated ImIL functionalized MSN@GO] NPs has more cytotoxic effect on MCF-7 as the cancerous model cell versus pure CUR. Consequently, the loading of CUR onto the PEGylated ImIL functionalized MSN@GO NPs is a considerable modification to overcome the short half-life and instability of CUR under normal conditions in order to raise the CUR capabilities to be utilized in the cancer therapy.

ACKNOWLEDGEMENTS

This research was supported by grants from the research councils of Tehran University of Medical Sciences and INSF (Iran National Science Foundation).

REFERENCES

- [1] Z. Gao, L. Zhang, J. Hu, Y. Sun, Mesenchymal stem cells: a potential targeted-delivery vehicle for anti-cancer drug loaded nanoparticles. *N.B.M.* 9 (2013) 174–184.
- [2] S.I. Stankovich, D.A. Dikin, G.H. Dommett, K.M. Kohlhaas, E.J. Zimney, E.A. Stach, R.D. Piner, S.T. Nguyen, R.S. Ruoff, Graphene-based composite materials. *Nature* 442 (2006) 282–286.
- [3] Q. Liu, J. Shi, J. Sun, T. Wang, L. Zeng, G. Jiang, Graphene and graphene oxide sheets supported on silica as versatile and high-performance adsorbents for solid-phase extraction, *Angew. Chem. Int. Ed. Engl.* 50 (2011) 5913–5917.
- [4] G.I. Xu, X. Chen, J. Hu, P. Yang, D. Yang, L. Wei, Immobilization of trypsin on graphene oxide for microwave-assisted on-plate proteolysis combined with MALDI-MS analysis, *Analyst.* 137 (2012) 2757–2761.
- [5] C. Shan, H. Yang, D. Han, Q. Zhang, A. Ivaska, L. Niu, Water-Soluble Graphene Covalently Functionalized by Biocompatible Poly-L-lysine, *Langmuir* 25 (2009) 12030–12033.
- [6] H. Dong, Z. Zhu, H. Ju, H. Yan, Triplex signal amplification for electrochemical DNA biosensing by coupling probe-gold nanoparticles–graphene modified electrode with enzyme functionalized carbon sphere as tracer, *Biosens. Bioelectron.* 33 (2012) 228–232.
- [7] A. Balaji, M.V. Vellayappan, A.A. John, A.P. Subramanian, S.K. Jaganathan, M. SelvaKumar, A.A. Mohd Faudzi, E. Supriyanto, M. Yusof, Biomaterials based nano-applications of Aloe vera and its perspective: a review, *RSC Adv.* 5 (2015) 72638–72652.
- [8] R.K. Maheshwari, A.K. Singh, J. Gaddipati, R.C. Srimal, Multiple biological activities of curcumin: a short review, *Life Sci.* 78 (2006) 2081–2087.
- [9] S.C. Gupta, S. Patchva, W. Koh, B.B. Aggarwal, Discovery of curcumin, a component of golden spice, and its miraculous biological activities, *Clin. Exp. Pharmacol. Physiol.* 39 (2012) 283–299.
- [10] P. Verderio, P. Bonetti, M. Colombo, L. Pandolfi, D. Prosperi, Intracellular drug release from curcumin-loaded PLGA nanoparticles induces G2/M block in breast cancer cells, *Bio. Mac. Molecules.* 14 (2013) 672–82.
- [11] L. Ma'mani, S. Nikzad, H. Kheiri-manjili, S. al-Musawi, M. Saeedi, S. Askarlou, A. Foroumadi, A. Shafiee, Curcumin-loaded guanidine functionalized PEGylated I3ad mesoporous silica nanoparticles KIT-6: Practical strategy for the breast cancer therapy, *Eur. J. Med. Chem.* 83 (2014) 646–654.
- [12] H. Kheiri Manjili, L. Ma'mani, S. Tavaddod, M. Mashhadikhan, A. Shafiee, H.D. Naderi-Manesh, L-Sulforaphane Loaded Fe₃O₄@ Gold Core Shell Nanoparticles: A Potential Sulforaphane Delivery System, *PloS one* 11 (2016) e0151344.
- [13] B.B. Aggarwal, A. Kumar, A.C. Bharti, Anticancer potential of curcumin: preclinical and clinical studies, *Anticancer Res.* 23 (2003) 363–98.
- [14] W.B. Liechty, D.R. Kryscio, B.V. Slaughter, N.A. Peppas, Polymers for drug delivery systems, *Annu. Rev. Chem. Biomol. Eng.* 1 (2010) 149–173.
- [15] A. Balaji, M.V. Vellayappan, A.A. John, A.P. Subramanian, S.K. Jaganathan, M. SelvaKumar, A.A. Mohd Faudzi, E. Supriyanto, M. Yusof, Biomaterials based nano-applications of Aloe vera and its perspective: a review, *RSC Adv.* 5 (2015) 86199–86213.
- [16] I.I. Slowing, B.G. Trewyn, S. Giri, V.S.Y. Lin, Mesoporous Silica Nanoparticles for Drug Delivery and Biosensing Applications, *Adv. Funct. Mater.* 17 (2007) 1225–1236.
- [17] X. Wang, Y. Pei, M. Lu, X. Lu, X. Du, Highly efficient adsorption of heavy metals from wastewaters by graphene oxide-ordered mesoporous silica materials, *J. Mater. Sci.* 50 (2015) 2113–2121.
- [18] H. Rao, X. Wang, X. Du, Z.H. Xue, The relationship between the hydrophobic capacity and extraction efficiency of organic–inorganic hybrid mesoporous silicas for the determination of dibutyl phthalate by SPME–HPLC, *J. Porous Mater.* 20 (2013) 1231.
- [19] B. Coasne, A. Galarneau, R.J.M. Pellenq, F. Renzo, Adsorption, intrusion and freezing in porous silica: the view from the nanoscale, *Chem. Soc. Rev.* 42 (2013) 4141–4171.
- [20] A. El-Safty Sherif, Organic–inorganic hybrid mesoporous monoliths for selective discrimination and sensitive removal of toxic mercury ions, *J. Mater. Sci.* 44 (2009) 6764–6774.

- [21] S. Khoee, H.B. Rahimi, Intermolecular interaction and morphology investigation of drug loaded ABA-triblock copolymers with different hydrophilic/lipophilic ratios. *Bioorg. Med. Chem.* 18 (2010) 7283–7290.
- [22] T.M. Allen, Ligand-targeted therapeutics in anticancer therapy, *Nat. Rev. Cancer* 2 (2002) 750–763.
- [23] K. Pal, S. Pore, S. Sinha, R. Janardhanan, D. Mukhopadhyay, R. Banerjee, Structure activity study to develop cationic lipid-conjugated haloperidol derivatives as a new class of anticancer therapeutics. *J. Med. Chem.* 54 (2011) 2378–2390.
- [24] S. Wang, E.E. Dormidontova, Nanoparticle design optimization for enhanced targeting: Monte Carlo simulations, *Biomacromolecules* 11 (2010) 1785–1795.
- [25] S. Khoee, R. Rahmatolahzadeh, Synthesis and characterization of pH-responsive and folated nanoparticles based on self-assembled brush-like PLGA/PEG/AEMA copolymer with targeted cancer therapy properties: A comprehensive kinetic study, *Eur. J. Med. Chem.* 50 (2012) 416–427.
- [26] M. Ashjari, S. Khoee, A.R. Mahdavian, R. Rahmatolahzadeh, Self-assembled nanomicelles using PLGA–PEG amphiphilic block copolymer for insulin delivery, a physicochemical investigation and determination of CMC values, *J. Mater. Sci. Mater. Med.* 23 (2012) 943–953.
- [27] T. Asefa, Z. Tao, Biocompatibility of Mesoporous Silica Nanoparticles, *Chem. Res. Toxicol.* 25 (2012) 2265–2284.
- [28] L. Ma'mani, S. Miri, M. Mahdavi, S. Bahadorikhalili, L. Lotfi, A. Foroumadi, A. Shafiee, Palladium catalyst supported on N-aminoguanidine functionalized magnetic graphene oxide as a robust water-tolerant and versatile nanocatalyst, *RSC Adv.* 4 (2014) 48613–48620.
- [29] E. Yoo, T. Okata, T. Akita, M. Kohyama, J. Nakamura, I. Hounma, Enhanced electrocatalytic activity of Pt subnanoclusters on graphene nanosheet surface, *Nano Lett.* 9 (2009) 2255–2259.
- [30] M. Mahdavi, H. Lijan, S. Bahadorikhalili, L. Ma'mani, P. Rashidi Ranjbar, A. Shafiee, Copper supported β -cyclodextrin grafted magnetic nanoparticles as an efficient recyclable catalyst for one-pot synthesis of 1-benzyl-1H-1,2,3-triazolodibenzodiazepinone derivatives via click Reaction, *RSC Adv.* 6 (2016) 28838–28843.